RSC Advances

ROYAL SOCIETY OF CHEMISTRY

www.rsc.org/advances

Journal Name

RSCPublishing

ARTICLE

New product from old reaction: uniform magnetite nanoparticles from iron-mediated synthesis of alkali iodides and their protection from leaching in acidic media

Cite this: DOI: 10.1039/x0xx00000x

Received 00th January 2012,
Accepted 00th January 2012

DOI: 10.1039/x0xx00000x

www.rsc.org/

R. P. Pogorilyi,[a] I. V. Melnyk,[a] Y. L. Zub,[a] S. Carlson,[b] G. Daniel,[c] P. Svedlindh,[d] G. A. Seisenbaeva[e]* and V. G. Kessler[*]

Iron-mediated synthesis of alkali metal iodides was quite unexpectedly demonstrated to be able to serve as a cost-efficient and reliable source of spherical single crystalline near-stoichiometric magnetite (Fe_3O_4) nanoparticles as revealed by TEM and XRD studies and also by XANES spectroscopic quantification of the Fe^{2+}-content. Using the particles as nuclei for the Stoeber synthesis of silica nanoparticles, core-shell magnetic material has been produced. The nature of the magnetic component was probed by XANES spectroscopy. The size of the particles is dependent on the synthesis conditions and Si:Fe ratio but can be kept below 100 nm. It is the Si:Fe ratio that determines the stability of the particles in acidic medium. The latter was investigated spectrophotometrically as leaching of Fe^{3+}-cations. Considerable stability was observed at Si:Fe > 10, while at Si:Fe ≥ 20 no measurable leaching could be observed in over 10 days. Magnetic nanoparticles with improved stability in acidic medium provide an attractive basis for creation of adsorbent materials for applications in harsh media.

Introduction

During the last decade magnetic nanoparticles have received increasing attention due to their broad and well established spectrum of high-tech applications. They have been used effectively as components in contrast media for nuclear magnetic resonance imaging[1,2] in advanced solutions for nanomedicine (including magnetically directed drug delivery vehicles[3,4] and materials for hyperthermia[4-6]), magnetically removable catalysts,[7] and, more recently, as magnetically removable adsorbents.[8-12] Several classes of chemically different substances found application as magnetic nanoparticles, including metals (in the first hand, iron and it's alloys[13-16]), simple and complex iron oxides,[17-19] and also gadolinium oxide, Gd_2O_3,[20] and gadolinium ferrite, $GdFeO_3$.[21] In many of these applications the problems of stability in relatively acidic media have been crucial for use of the particles. . In search for highly magnetic particles for use in biomedicine, metal particles composed either of alloys with noble metals or having core-shell structures with a noble metal shell have been studied.[22] Only magnetite, Fe_3O_4, nanoparticles are currently approved by FDA for such applications as Feridex I.V. formulation. Commonly applied FDA approved alternatives are soluble chelates of gadolinium. In other, potentially broader scale industrial applications, current focus is also set on magnetite in the view of its environmentally benign character and magnetic properties staying in a well investigated relation to the size and morphology of its crystals.[23-25].

A broad spectrum of synthetic approaches to magnetite nanoparticles has been developed, comprising, mostly, co-precipitation in aqueous media[26], but also solvothermal decomposition of iron acetylacetonates or alkoxides in different solvents (i.e. xylene,[27] oleylamine or oleyl alcohol,[28] di-, tri- or tetraethylene glycol,[29] acetophenone [30] etc.), Pechini synthesis [31] and related processes followed by thermal treatment or autocombustion,[32] etc. More recently also a microemulsuion method[33], microwave [19] and ultrasonic [34] approaches, and polymer templation have been proposed.[35] Generally the nucleation of iron oxides, particularly magnetite, is a facile process that can with advantage be carried out by a template- and surfactant-free processes. Major challenges are however, the relatively easy aggregation of the particles as well as their relatively high sensitivity to oxidation, which is often associated with partial or complete loss of the magnetic properties.[36] Etching and re-dissolution, which were often observed but to the best of our knowledge never have been fully quantified, are also well known problems even in biomedical applications where even the pH in the cytosol relatively close to neutral (4.5-5.5) has been recognized as potential hazard for long-term application of the particles.[37]
Elegant approaches dealing with production of alloys with noble metals or construction of a shell consisting of a noble metal [22] are because of cost reasons not viable outside medicine and the creation of polymer [38] or silica shells [39] have been broadly recognized as the most promising routes to stabilization of magnetite nanoparticles. Silica shells are most promising in view of their chemical and especially thermal stability. Several

approaches have been proposed for producing silica layers on the surface of magnetite with sol-gel and specifically Stoeber technique being most popular. Also microemulsion and reverse microemulsion syntheses have been tested for this purpose.
In the present paper we intended to bring answers to two principal challenges in developing magnetic nanoparticles for broad scale industrial applications by (i) identification of an industrial process capable to offer iron oxide nanoparticles as a cheap byproduct, thereby principally improving their accessibility, and (ii) determination of the parameters providing iron oxide core – silica shell nanoparticles with enhanced stability in acidic media, confirmed by quantitative analysis of iron leaching, thus permitting potential repeated extraction and re-use of the nanoparticles.

Results and discussion

Materials in the form of nanoparticles are usually quite expensive to produce, store and handle due to their specific production conditions and in many cases considerable chemical sensitivity to environment. The iron oxide and in particular magnetite nanoparticles (Fe_3O_4) can undergo undesired transformations on oxidation in ambient conditions, but are relatively stable when they possess high crystallinity and if their size exceeds ca 10 nm.[30] Magnetite is eagerly generated in nano form in many processes in nature and it appeared reasonable to seek possibility for obtaining it as byproduct in processes aimed at other high purity chemicals. An interesting source for such a process is the iron iodide route to alkali iodides, applied in production of iodides for food and pharmaceutical purposes. Here, the large scale technology based on interaction of alkali hydroxides with elementary iodine fails to produce salts with sufficient purity.[40] The chemical reactions behind the process are described in [41]:

$$\mathbf{3Fe(s) + 4I_2(aq) \longrightarrow Fe_3I_8(aq)}$$

$$\mathbf{Fe_3I_8(aq) + 4Na_2CO_3 \longrightarrow Fe_3O_4(s) + 8NaI(aq) + 4CO_2(g)}$$

The magnetite generated in this process to the best of our knowledge has never been characterized. Even the nature and composition of the assumed mixed-valence iron iodide intermediate, Fe_3I_8, seemed to be a mere assumption based on the data for its structurally characterized fluoride analog, Fe_3F_8.[42] The process in itself is facile and reproducible, easy to model under laboratory conditions.
The separated solid was an extremely fine black powder easily re-dispersible in both aqueous and alcohol medium. It consisted by TEM observation of (partly aggregated) but surprisingly uniform spherical particles with average diameter about 16 nm (see Fig. 1). This value correlates well with the domain size calculated using Debye-Scherrer formula from the X-ray diffraction data on material washed with hydrochloric acid (see Fig. 1).
It should be noted that this latter step is important as the primary product of the reaction contains distinctly an admixture of the siderite $FeCO_3$ phase. Washing with acid removes the siderite phase and causes distinct decrease in the particle size (from ca 20 nm), as can be noticed from line broadening in the XRD pattern.

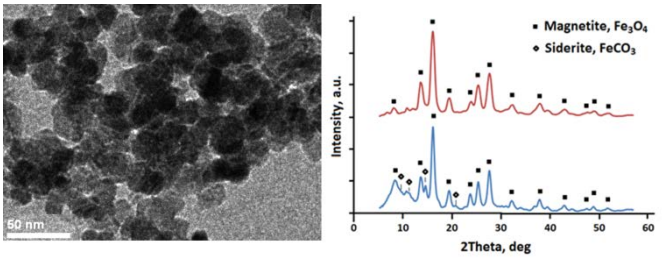

Figure 1. TEM image of typical Fe_3O_4 nanoparticles produced by iodide route (left) and the XRD patterns of the as-precipitated iron oxide from the iodide route (below right) and the one washed with 0.1 M HCl (above right).

An important parameter demonstrating the potential quality of a magnetite related phase is its content of iron(II) cations. The loss of Fe(II) is the most apparent indicator of oxidation, transforming magnetite into first the less magnetic maghemite phase γ-Fe_2O_3 and then finally into completely non-magnetic hematite, α- Fe_2O_3. Quantification of Fe(II) is usually quite a challenging task. Magnetite and maghemite phases are iso-structural, which makes XRD impossible to use for this purpose. Raman spectroscopy permits to distinguish pure maghemite from magnetite, but is difficult to use for quantification of the oxidation extent.[30] The latter can be carried out either by Mössbauer spectroscopy or by a XANES (X-ray Adsorption Near Edge Structure) spectroscopy, exploiting the intensity of pre-edge signal associated with Fe^{2+}-cations. In the present work the iron(II) content was estimated by XANES using stoichiometric magnetite $Fe^{II}Fe^{III}{}_2O_4$ produced in nitrogen atmosphere by standard co-precipitation from Fe^{2+} and Fe^{3+} salt solutions [26] as etalon for 100% Fe^{2+} and pseudobrukite, Fe_2TiO_5, synthesized hydrothermally from Fe^{3+} solution and titanium methoxide [43] as the standard for Fe^{2+}-free phase. The content of iron(II) in the phase produced by iodide route was always exceeding 90%, indicating that the exploited approach is offering close-to-stoichiometry Fe_3O_4 nanoparticles (see Fig. 2).

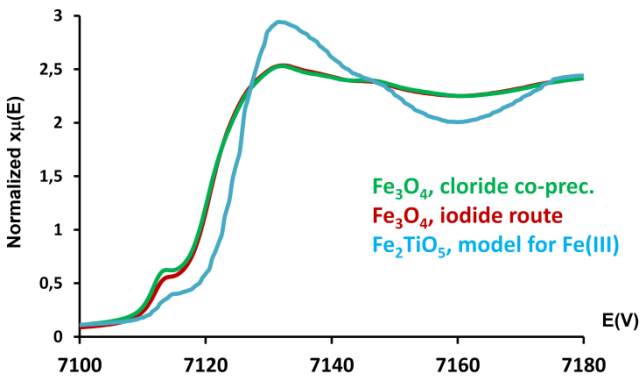

Figure 2. Normalized XANES spectra of the Fe_3O_4 produced by iodide route compared to standard stoichiometric material and with Fe_2TiO_5 containing only Fe^{3+}-cations.

Surface protection of the nanoparticles was achieved through deposition of a silica layer using Stöber methods, hydrolysis-polycondensation of TEOS in ethanol-ammonia solutions (see Fig. 3).[44] The produced powders were brown in color and apparently remained magnetic.

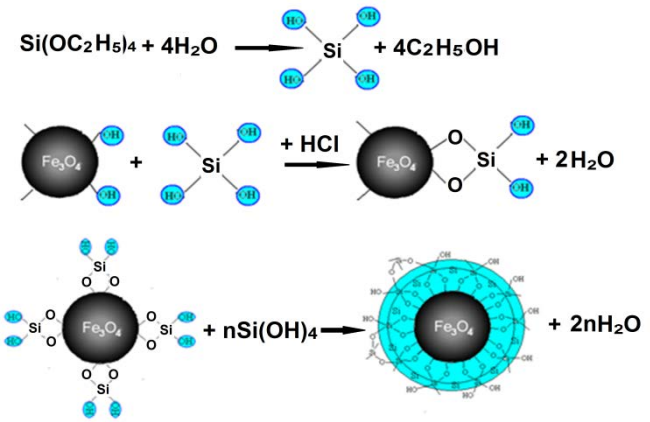

Figure 3. The general scheme for construction of a silica shell on the surface of iron oxide particles.

The SEM images of the produced core-shell materials shown in Fig. 4 reveal particles with spheroidal shape. Their size increases with the decrease in the Fe_3O_4:SiO_2 ratio under the same synthetic conditions.

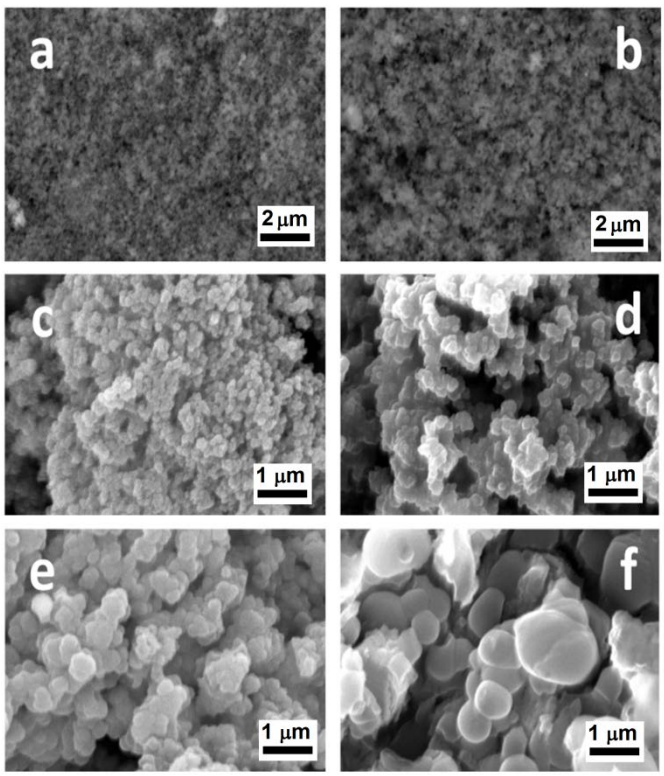

Figure 4. SEM micrographs of functionalized magnetite materials with Fe_3O_4:SiO_2 ratios 1:2.5 (a), 1:5 (b), 1:10 (c), 1:20 (d), 1:30 (e), 1:45 (f).

Thus for the samples with Fe_3O_4:SiO_2 = 1:10 the average particle size was ~50 nm, the samples with Fe_3O_4:SiO_2 = 1:20 ~100 nm, those with Fe_3O_4:SiO_2 = 1:30 ~300 nm, and for the samples with Fe_3O_4:SiO_2 = 1:45 ~500 nm. It has to be mentioned that for the Fe_3O_4:SiO_2 ratios less than 1:10 an extensive coalescence of the particles was observed.

TEM observations revealed that the particles identified in the SEM images consist of small aggregates (Fig. 5). Their nuclei contain apparently partially aggregated iron oxide nanoparticles easily distinguishable due to their higher electron density (i.e. darker colour).

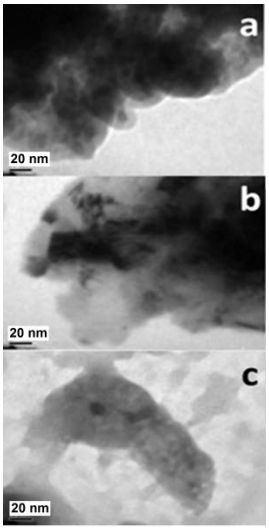

Figure 5. TEM micrographs of functionalized magnetite materials with Fe_3O_4:SiO_2 ratios 1:10 (a), 1:30 (b), 1:45 (c).

Formation of the silicon oxide layer on the surface of the particles can easily be followed by IR spectroscopy (Fig. 6). In the spectra of all produced core-shell samples a broad band corresponding to ν_{as}(SiOSi) vibrations is well visible in the 1000-1200 cm^{-1} region. At higher wavenumbers a characteristic shoulder typical of the spectra of siloxane layers was visible. Other characteristic bands were ν(FeO) at 550-650 cm^{-1} and δ(H_2O) at 1635-1645 cm^{-1}. Strong broad ν(OH) band at over 3100 cm^{-1} testifies the presence of adsorbed water.

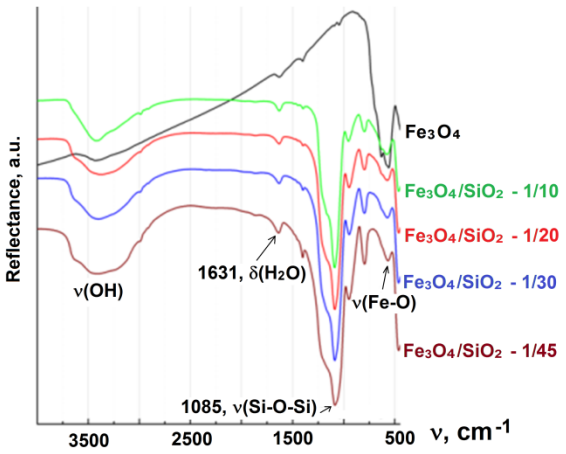

Figure 6. DRIFT spectra of the functionalized magnetite samples.

Analysis of the XRD patterns of core-shell materials showed in all cases the presence of spinel phase structurally related to Fe_3O_4. The diffractograms of both the initial magnetite and the derived composite materials (see Fig. 7) contain characteristic reflections at d(hkl) 4.8474(111), 2.9684(220), 2.5315(311), 2.4237(222), 2.0990(400), 1.6158(511), and 1.4842(440) Å. Their intensity decreases on the increase in the SiO_2 content, while the intensity of the amorphous halo at lower 2Θ increases. The line width for the peaks corresponding to iron oxide and their position stay practically unchanged, which might be considered as indication that the core material remains in the form of magnetite.

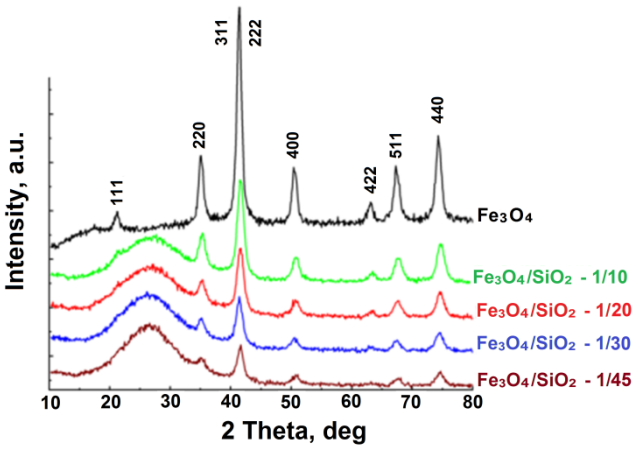

Figure 7. Diffractogram of the original magnetite and the derived FeO_x@SiO_2 core-shell materials.

Insight into the chemical transformation of the iron oxide in the course of synthesis of the core-shell material was obtained using XANES spectroscopy (see Fig. 8). Growth of the surface SiO_2 layer occurs in the basic medium, favouring oxidation of Fe^{2+} into Fe^{3+}.

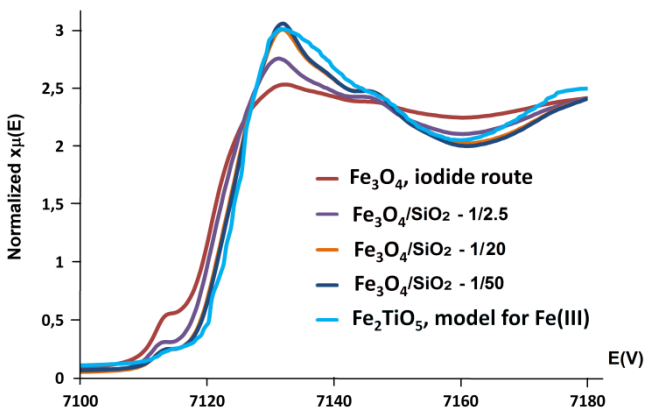

Figure 8. Normalized XANES spectra of the Fe_3O_4 & SiO_2 core-shell materials with different thickness of the shell compared to Fe_3O_4 produced by iodide route to Fe_2TiO_5 containing only Fe^{3+}-cations.

The larger the amount of silica to be added the longer is the process duration until completion and the deeper the oxidation of the original magnetite phase. Already for the tentative ratio Fe_3O_4:SiO_2 ≤ 1:20 the core material has the content of Fe^{2+} reduced by about 80% and thus is no longer magnetite Fe_3O_4, but predominantly maghemite, γ-Fe_2O_3. There is no visible transformation into non-magnetic hematite and the material remains strongly magnetic, permitting for effective removal of the material from solution by magnet.

Figure 9 shows magnetic hysteresis loops at 300 K for the original iron-oxide powder and the iron oxide core – silica shell nanoparticles. Both samples exhibit zero coercivity and a superparamagnetic behavior at 300 K.

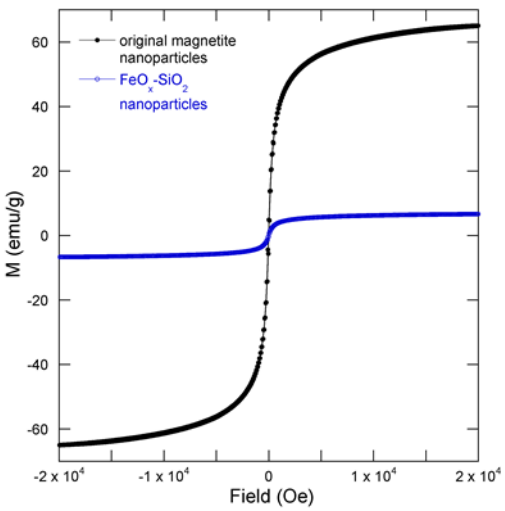

Figure 9. Magnetization versus field at T = 300 K for the original iron-oxide nanopowder (black symbols) and the iron oxide core – silica shell (blue symbols) Fe_3O_4:SiO_2 = 1:20 nanoparticles.

The saturation magnetization of the magnetite nanoparticles themselves is 65 emu/g at 300 K, which is rather high in comparison with magnetic characteristics usually obtained for nanosized magnetite produced by co-precipitation[45] or by solvothermal synthesis[30] and is even comparable to the saturation magnetization in bulk magnetite, which is 92 emu/g.[46] Since the encapsulation of the iron oxide particles is associated with their oxidation to maghemite and some loss in magnetic characteristics, it can be deduced that the content of iron oxide has to be estimated to over 10 wt% for the chemically stable composite nanoparticles, which is in good agreement with the observed saturation magnetization (6 emu/g for Fe_3O_4:SiO_2 = 1:20). The magnetic extraction in a test-tube (5 mg particles in 2 ml water) was completed typically in 30 seconds (see Fig. FS2 and provided supplementary video).

In the view that the produced materials are containing mainly Fe^{3+}-cations, it appeared logical to use for quantifying of iron leaching the technique visualizing the concentration of iron(III). To investigate the stability of the produced core-shell particles they were subjected to leaching in 0.1 M nitric acid containing excess of potassium thiocyanate which formed a strongly red-coloured complex with the Fe^{3+}-cations. Dissolution of non-functionalized magnetite was also studied for comparison under

the same conditions. It turned out that the magnetite material itself lost 80% of iron within 48 h (see Fig. 10).

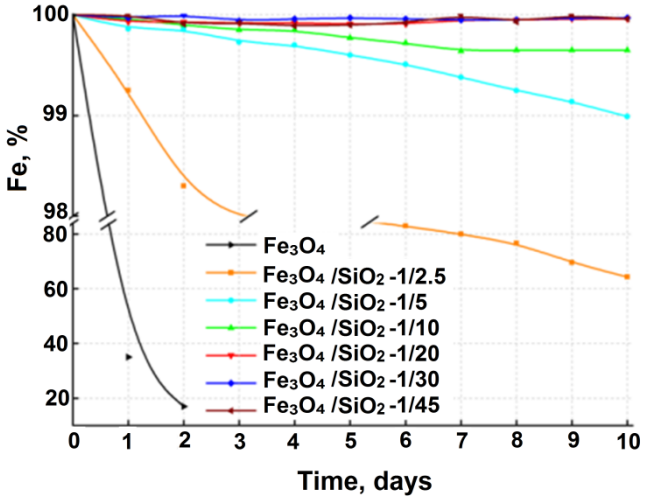

Figure 10. Leaching of iron from pure Fe_3O_4 and the Fe_3O_4 & SiO_2 core-shell materials

Core-shell particles with Fe_3O_4:SiO_2 = 1:2.5 lost within the same time only 1.5% of their weight within the same time and 38% within 10 days. Leaching of iron from the samples with Fe_3O_4:SiO_2 = 1:5 within 10 days reaches only 1%, and for the sample with Fe_3O_4:SiO_2 = 1:10 is less than 0.5%. No measurable leaching could be observed for the samples with even higher silica content, which demonstrates that these materials possess practically unlimited stability in acid.

Experimental

All experiments were carried out at ambient atmosphere. The chemicals: iron powder (STREM), sublimed elementary iodine (STREM), 25% ammonia (VWR), tetraethoxysilane, $Si(OC_2H_5)_4$ (TEOS, Aldrich, 98%); ethanol (Solveco, 96%); acetone (Aldrich); $Fe(NO_3)_3{\times}9H_2O$, KCNS, NH_4F (98%, Fluka); were used as received. 0.1M HCl, 0.1M HNO3 and 0.1M Na_2CO_3 or K_2CO_3 (VWR) were produced from concentrated solutions or pure solid salts by dilution/dissolution.

Synthetic procedures

Preparation of magnetite nanoparticles. The experimental setup modeling industrial techniques for the synthesis of alkali iodides[41] has been made as follows: first, iron metal powder was dissolved in warm water solution (80°C) in the presence of stoichiometric amounts of elementary iodine for the formation of a Fe_3I_8 intermediate. The reddish brown solution was removed from eventual rests of unreacted iron powder and transferred in a vessel connected to a funnel containing stoichiometric quantity of alkali carbonate solution. Carbonate solution was added dropwise under constant stirring. The black precipitate formed was separated by sedimentation, washed first with a small portion of 0.1 M HCl followed by water and alcohol and finally dried in air.

Preparation of core-shell material. Magnetite nanoparticles were coated by silica using Stoeber technique[44]: 100 mg Fe_3O_4 were dispersed in 40 ml ethanol on stirring in 10 min and then 20 ml of 25% aqueous ammonia solution was added. Thereafter, the required amount of TEOS was added slowly (0.05 ml each 10 min) within 3 h on constant stirring. Molar ratio between Fe_3O_4 and SiO_2 in resulting material was varied from 1:2.5 to 1:45. Final dispersion was kept on constant stirring for additional 30 min. The produced solid was separated from solution by precipitation overnight and washed then with deionized water several times. The obtained wet material was re-dispersed in 25 ml ethanol and subjected to sonication in 3 min. The solid was separated by sedimentation and the whole washing procedure was repeated 2 more times. Finally the material was dried in vacuum for 1 h at room temperature, 1 h at 50°C and 4 h at 100ºC.

Characterization methods.

The leaching tests were performed with 5 mg of each sample of pure or SiO_2-coated magnetic iron oxide in 10 ml 0.1 M HNO_3 on addition of 0.1 g of KSCN. Determination of iron content on leacheate was carried out spectrophotometrically with a Thermo scientific Genesys 20 instrument using thiocyanate ions as complexing colorant.[47] Calibration was carried out with stock solutions of iron(III) nitrate in 0.1 M HNO_3 and standard excess of potassium thiocyanate. The produced stock solution was diluted to the desired concentration and the optical density was measured to construct the calibration curve (see Supplementary Fig FS1). The obtained calibration was tested on storage to confirm the stability of produced solutions with time.

The DRIFT spectra were recorded on the Thermo Nicolet Nexus FT-IR at 8 cm^{-1} resolution using the Spectra Tech collector diffuse reflectance accessory at room temperature. The samples were mixed with KBr (1:30) and were used to fill the DRIFT sample cup before measurements.

The nitrogen adsorption isotherms for all the samples were measured on a "Kelvin-1042" adsorption analyzer (Costech Microanalytical). Before the measurements, the samples were out gassed at 383 K in the helium atmosphere. The BET specific surface area[48] was calculated in the relative pressure range between 0.05 and 0.35.

SEM images of the samples were obtained using JSM 6060LA (Jeol, Tokyo, Japan) scanning electron microscope in secondary electron mode at cathode voltage of 30.00 kV. The samples were deposited on carbon tape. For improved imaging and charge reduction the samples were coated by gold using sputtering technique.

X-ray diffraction study of the iron oxide samples were carried out with Bruker SMART Apex-II multifunctional diffractometer using MoKα radiation (λ = 0.71073 Å). Bruker Apex-II program package was used for data collection and reduction and the EVA-12 program was applied for phase identification and indexing. The XRD of the core-shell particles was investigated with DRON-UM1 diffractometer with Bragg-Brentano acquisition setup using Co K_α radiation (λ = 1,79021 Å) with Fe foil filter for the reflected beam.

Magnetization measurements were performed in a Lake Shore 7400 series vibrating sample magnetometer. Isothermal magnetization measurements were performed at 300 K; the magnetization versus applied field was measured in the field range ±20000 Oe. The mass magnetization is in this work

defined with respect to weight of iron oxide core – silica shell nanoparticles.

Iron K edge X-ray absorption spectra were recorded at the wiggler beam line I811, MAX IV Laboratory, Lund, Sweden.[49] The station was equipped with a Si (111) double crystal monochromator. XANES data collection was performed in fluorescence mode using a Stern-Heald-Lytle type detector[50] equipped with a Canberra Industries Inc. PIPS photo diode. The primary beam flux, in a beam-spot size of 1 x 2 mm^2, was approximately 1011 photons/seconds. Higher-order harmonics were reduced by detuning the second monochromator crystal to 30 % of maximum intensity. The energy scale of the X-ray absorption spectra were calibrated by assigning the first inflection point of the K edge of an iron foil to 7712 eV.[51] The IFEFFIT program package[52] was used for the data treatment.

Conclusions

The present work has shown that byproducts from the iron-mediated synthesis of alkali iodides can successfully act as a source of good quality magnetite nanoparticles for application in the synthesis of magnetic hybrid nanomaterials. Coating of the magnetite particles with silica layers using the Stöber reaction is associated with considerable oxidation of the initial magnetite into maghemite, but the resulting iron oxide conserves its spinel structure and good magnetic properties. Using silica shell with a silica content Fe_3O_4:SiO_2 = 1:20 and higher guarantees unlimited stability of the core-shell particles in strongly acidic medium. The cheap and stable nanomaterials developed in this work have potential to broaden applications of magnetic nanoparticles on broad industrial scale in areas associated with harsh process conditions as, for example in hydrometallurgy.

Acknowledgements

The financial support from the EU FP-7 Program Project "Sustainable exploitation of the Rare Earth Element Resources in Europe (EURARE)" and from the Swedish Research Council Swedish Research Links Program Project "Multifunctional magnetically removable adsorbents" (Grant 2012-9772-98229-17) is gratefully acknowledged. The authors express their gratitude to Sofia Kontos for help with the carrying out of magnetic measurements.

Notes and references

[a] Chuiko Institute of Surface Chemistry, National Academy of Sciences of Ukraine, 17, General Naumov Street, Kyiv 03164, Ukraine.

[b] MAX IV Laboratory, Lund University, P.O Box 118, 22100 Lund, Sweden.

[c] Department of Forest Products, Swedish University of Agricultural Sciences, Box 7008, 75007 Uppsala, Sweden.

[d] Solid State Physics, Department of Engineering, Uppsala University, Box 534, SE-751 21 Uppsala, Sweden.

[e] Department of Chemistry and Biotechnology, Swedish University of Agricultural Sciences, Box 7015, 750 07 Uppsala, Sweden.

Electronic Supplementary Information (ESI) available: [details of spectrophotometric measurements]. See DOI: 10.1039/b000000x/

1 D. Maity, P. Chandrasekharan, C.T. Yang, K.H. Chuang, B. Shuter, J.M. Xue, J. Ding and S.S. Feng, *Nanomedicine*, 2010, **5**, 1571–1578.

2 M. Brähler, R. Georgieva, N. Buske, A. Müller, S. Müller, J. Pinkernelle, U. Teichgräber, A. Voigt and H. Bäumler, *Nano. Lett*., 2006, **6**, 2505–2509.

3 O. Veiseh, J.W. Gunn and M. Zhang, *Adv. Drug Deliv. Rev*., 2010, **62**, 284-304.

4 S. Guo, D. Li, L. Zhang, J. Li and E. Wang, *Biomaterials*, 2009, **30**, 1881–1889.

5 J. Puig, C.E. Hoppe, L.A. Fasce, C.J. Perez, Y. Pineiro-Redondo, M. Banobre-Lopez, M.A. Lopez-Quintela, J. Rivas and R.J.J. Williams, *J Phys Chem C*, 2012, **116**, 13421-13428.

6 D.L. Zhao, X.W. Zeng, Q.S. Xia and J.T. Tang, *J. Alloys Comp*., 2009, **469**, 215–218.

7 T. Tang, H. Fan, S. Ai, R. Han and Y. Qui, *Chemosphere*, 2011, **83**, 255-264.

8 M. Khajeh, S. Laurent and K. Dastafkan, *Chem. Rev*., 2013, **113**, 7728-7768.

9 A. Akbarzadeh, M. Samiei and S. Davaran, *Nanoscale Research Letter*, 2012, **7**, 144-156.

10 M.E. Mahmoud, M.S. Abdelwahab and E.M. Fathallah, *Chem. Eng. J*,. 2013, **223**, 318–327.

11 R.P. Pogorilyi, I.V. Melnyk, Y.L. Zub, G.A. Seisenbaeva, V.G. Kessler, M.M. Shcherbatyik, A. Košak and A. Lobnik, *J. Sol-Gel Sci.Tech*., 2013, **68**, 447–454.

12 A. Pourjavadi, S.H. Hosseini, F. Seidi and R. Soleyman, *Polym. Int*., 2013, **62**, 1038–1044.

13 M. Chen, S. Yamamuro, D. Farrell and S.A. Majetich, *J. Appl. Phys*., 2003, **93**, 7551-7553.

14 R. Fernández-Pacheco, M.R. Ibarra, J.G. Valdivia, C. Marquina, D. Serrate, M.S. Romero and M. Gutiérrez, *J. Arbiol. NanoBiotech*., 2005, **1**, 300-303.

15 H. Zeng, J. Li, Z.L. Wang, J.P. Liu and S.H. Sun, *Nano Lett*., 2004, **4**, 187-190.

16 A. Figuerola, A. Fiore, R.D. Corato, A. Falqui, C. Giannini, E. Micotti, A. Lascialfari, M. Corti, R. Cingolani, T. Pellegrino, P.D. Cozzoli and L. Manna, *J. Am. Chem. Soc*., 2008, **130**, 1477-1487.

17 K.S.M. Salih, P. Mamone, G. Dörr, T.O. Bauer, A. Brodyanski, C. Wagner, M. Kopnarski, R.N. Klupp Taylor, S. Demeshko, F. Meyer, V. Schünemann, S. Ernst, L.J. Gooßen and W.R. Thiel, *Chem. Mater*., 2013, **25**, 1430-1435.

18 L.H. Reddy, J.L. Arias, J. Nicolas and P. Couvreur, *Chem. Rev*., 2012, **112**, 5818−5878.

19 R. Pązik, E. Piasecka, M. Małecka, V.G. Kessler, B. Idzikowski, Z.;Śniadecki and R.J. Wiglusz, *RSC Adv*., 2013, **3**, 12230-12243.

20 F. Söderlind, H. Pedersen, R.M. Petoral, P.O. Käll and K. Uvdal, *J. Coll. Interf. Sci*., 2005, **288**, 130-148.

21 F. Söderlind, L. Selegård, P. Nordblad, K. Uvdal and P.O. Käll, *J. Sol-Gel Sci. Tech*., 2009, **49**, 253-259.

22 *Magnetic Nanoparticles: From Fabrication to Clinical Applications* (Ed. N.T.K. Thanh, 2012, CRC Press, London.

23 D.L. Zhao, X.W. Zeng, Q.S. Xia and J.T. Tang, *J. Alloys Comp*., 2009, **469**, 215–218.

24 W.D. Zhang, H.M. Xiao, L.P. Zhu and S.Y. Fu, *J. Alloys Comp*., 2009, **477**, 736–738.
25 M. Sangermano, P. Allia, P. Tiberto, G. Barrera, F. Bondioli, N. Florini and M. Messori, *Macromol. Chem. Phys*., 2013, **214**, 508−516.
26 R. Massart and V. Cabuil, *J. Chem. Phys*., 1987, **84**, 967–973.
27 A. Ahniyaz, G.A. Seisenbaeva, V.G. Kessler, L. Häggström, S. Kamali, C. Johansson and L. Bergström, *J. Magnetism Magnet. Mater*., 2008, **320**, 781-787.
28 D. Maity, S.G. Choo, J.B. Yi, J. Ding and J.M. Xue, *J. Magn. Magn. Mater*., 2009, **321**, 1256–1259.
29 H. Qu, S. Tong, K.J. Song, H. Ma, G. Bao, S. Pincus, W.L. Zhou and C. O'Connor, *Langmuir*, 2013, **29**, 10573−10578.
30 K.E. Wilkinson, B. Ekstrand-Hammarström, L. Ahlinder, K. Guldevall, R. Pazik, L. Kępiński, K.O. Kvashnina, S. Butorin, H. Brismar, B. Önfelt, L. Österlund, G.A. Seisenbaeva and V.G. Kessler, *Nanoscale*, 2012, **4**, 7383-7393.
31 H.Z. Qi, B. Yan, W. Lu, C.K. Li and Y.H. Yang, *Current Nanosci*., 2011, **7**, 381-388.
32 J.C. Aphesteguy, S.E. Jacobo, N.N. Schegoleva and G.V. Kurlyandskaya, *J. Alloys Comp*., 2010, **495**, 509–512.
33 C. Okoli, M. Sanchez-Dominguez, M. Boutonnet, S. Järås, C. Civera, C. Solans and G.R. Kuttuva, *Langmuir*, 2012, **28**, 8479−8485.
34 S. Wu, A. Suna, F.Q. Zhai, J. Wang, W.H. Xu, Q. Zhang and A.A. Volinsky, *Mater. Lett*., 2011, **65**, 1882-1884.
35 N. Phutthawong and M. Pattarawarapan, *Polym. Bull*., 2013, **70**, 691–705.
36 J. Tang, M. Myers, K.A. Bosnick, L.E. Brus, *J. Phys. Chem. B*, 2003, **107**, 7501-7506.
37 S. Begin-Colin, D. Felder-Flesch, in *Magnetic Nanoparticles from Fabrication to Clinical Applications*, N.T.K. Thanh Ed., CRC Press, 2012, P. 151-194.
38 S.R. Wan, J.S. Huang, H.S. Yan and K.L. Liu, *J. Mater. Chem*., 2006, **16**, 298–303.
39 A. Jitianu, M. Raileanu, M. Crisan, D. Predoi, M. Jitianu, L. Stanciu and M. Zaharescu, *J. Sol-Gel Sci.Tech*., 2006, **40**, 317–323.
40 A. Osol, J. Anderson and J. Hoover, *Potassium Iodide USP. Remington's Pharmaceutical Science: A Treatise on the Theory and Practice*, 15th ed., 1975.
41 Chinese patent CN202343189 U.
42 E. Herdtweck, *Z.Anorg.Allg.Chem*., 1983, **501**, 131-135.
43 G.A. Seisenbaeva, G. Daniel, J.M. Nedelec, Y.K. Gun'ko and V.G. Kessler, *J. Mater. Chem*., 2012**, 22**, 20374-20380.
44 W. Stöber and A. Fink, *J. Colloid Interface Sci*., 1968, **26**, 62-69.
45 C.N. Shauo, C.G. Chao and M.C. Cheng, *Mater. Trans*., 2006, **47**, 143-148.
46 D.H. Han, J.P. Wang and H.L Luo. *J. Magn. Magn. Mater*. **1994**, **136**, 176–182.
47 Y.Y. Lurie, *Analytical chemistry of industrial wastewater*. Chemistry. Moscow, 1984 (in Russian).
48 J.S. Brunauer, P.H. Emmet and E. Teller, *J. Am. Chem. Soc*., 1938, **60**, 309–319.
49 S. Carlson, M. Clausen, L. Gridneva, B. Sommarin and C. Svensson, *J. Synchrotron. Rad*., 2006, **13**, 359-364.
50 E.A. Stern and S.M. Heald, *Rev. Sci. Instrum*., 1979, **50**, 1579-1582.
51 A. Thompson, D. Attwood, E. Gullikson, M. Howells, K.J. Kim, J. Kirz, J. Kortright, I. Lindau, P.Pianatta, A. Robinson, J. Scofield, J. Underwood, D. Vaughan, G. Williams and H. Winick, *X-ray Data Booklet*, Berkeley, California, 2001**,** 94720.
52 M. Newville, *The IFEFFIT Reference Guide*. University of Chicago, Chicago, IL. Version 1.2., 2004.

Journal Name RSCPublishing

ARTICLE

TOC

Magnetic material stable to acid leaching was produced by silica coating of byproduct from the industrial synthesis of alkali iodides.

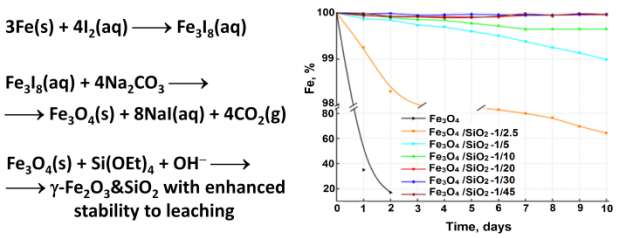

$3Fe(s) + 4I_2(aq) \longrightarrow Fe_3I_8(aq)$

$Fe_3I_8(aq) + 4Na_2CO_3 \longrightarrow$

$\longrightarrow Fe_3O_4(s) + 8NaI(aq) + 4CO_2(g)$

$Fe_3O_4(s) + Si(OEt)_4 + OH^- \longrightarrow$

$\longrightarrow \gamma\text{-}Fe_2O_3\&SiO_2$ with enhanced stability to leaching

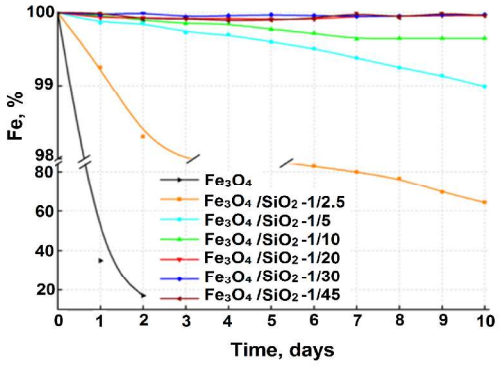

1079x398mm (96 x 96 DPI)